UNCLASSIFIED

Defense Technical Information Center
Compilation Part Notice

ADP011236

TITLE: Electro-Optically Modulated Biomolecular-Interaction Analysis Sensor

DISTRIBUTION: Approved for public release, distribution unlimited

This paper is part of the following report:

TITLE: Optical Sensing, Imaging and Manipulation for Biological and Biomedical Applications Held in Taipei, Taiwan on 26-27 July 2000. Proceedings

To order the complete compilation report, use: ADA398019

The component part is provided here to allow users access to individually authored sections of proceedings, annals, symposia, etc. However, the component should be considered within the context of the overall compilation report and not as a stand-alone technical report.

The following component part numbers comprise the compilation report:
ADP011212 thru ADP011255

UNCLASSIFIED

Electro-optically modulated biomolecular-interaction analysis sensor

Yao Cheng*[a], Yi-ren Chang[b], Che-hsin Lin[a], Long Hsu[b], Minking K. Chyu[c]

[a]Synchrotron Radiation Research Center

#1, R&D Road VI, Science-based Industrial Park, 30077, Hsinchu, Taiwan

[b]Department of ElectroPhysics, National Chiao-Tung University, Hsinchu, Taiwan

[c]Department of Mechanical Engineering, University of Pittsburgh, PA 5261, USA

ABSTRACT

This paper focuses on developing the platform technology of real-time biomolecular-interaction analysis (BIA) sensor chips. A detection scheme using the electro-optically modulated surface plasmon resonance (SPR) is suggested to advance the sensor features in reducing measurement complexity and time. The SPR method of a BIA sensing system detects slight changes of refractive index due to the biomolecular interaction at the solid-liquid interface. The most sensitive interrogation method among the possible conventional schemes is to measure the SPR angle of the attenuated total reflection. The electro-optical modulation replaces the mechanism of angle measurement not only to increase the speed but also to reduce the size. Recent progress of the multilayer SPR provides an effective mean of tailoring the microchip. Several multilayer configurations have been studied in this paper to realize the electro-optical SPR sensing. Especially, the long-range mode of surface plasmon was investigated to achieve the high-resolution and high-sensitivity detection.

Keywords: Biosensor, biomolecular-interaction analysis sensor, optical sensor, surface plasmon resonance, electro-optical modulation, multilayer.

NOMENCLATURE

BIA Biomolecular-interaction analysis
SPR Surface plasmon resonance
EO Electro-optical
ATR Attenuated total reflection
ω Frequency of the electromagnetic oscillation
ω_P Plasmon frequency of the metal
c Speed of light
k_0 Propagation constant of the incident light in vacuum
k_{SP} Propagation constant of the surface plasmon
k_R Real part of k_{SP}
k_I Imaginary part of k_{SP}
ε_m Complex dielectric constant of the metal
ε_R Real part of ε_m
ε_I Imaginary part of ε_m
ε_a Real dielectric constant the dielectric medium a
ε_b Real dielectric constant the dielectric medium b
d Thickness of the metal stab
γ_m Extinction coefficient of the field in the metal
γ_a Extinction coefficient of the field in the dielectric a
R Reflectivity
min Minimal reflection intensity at the resonance
curv Curvature of the reflection intensity at the resonance
θ Incident angle
θ_R Resonance angle
S_P Sampling sensitivity
S_S Steering sensitivity
n_P Refractive index of the sample layer
n_S Refractive index of the steering electro-optical layer
f_m Frequency of the EO modulation

* Correspondence: E-mail: Yao@mail.srrc.gov.tw Telephone: +886-35-780281ext 7309, Fax: +886-35-789816

In *Optical Sensing, Imaging, and Manipulation for Biological and Biomedical Applications*, Robert R. Alfano, Ping-Pei Ho, Arthur E. T. Chiou, Editors, Proceedings of SPIE Vol. 4082 (2000) • 0277-786X/00/$15.00

1. INTRODUCTION

ATR has been used to determine the optical constants of thin film samples for more than three decades[1]. Liedberg *et al*[2] introduced the BIA application of the SPR sensors in 1983. Instead of directly measuring the refraction index of samples by methods such as ellipsometry and reflectometry, the ATR generates an evanescent wave into the liquid phase to probe the sample interaction immobilized on the metal-liquid interface. The metal film is typically 50nm-thick Au or Ag for providing the optimum permittivities in the near IR and visible region[1]. The surface plasmon, a charge density wave propagating along the interface between metal and dielectric, absorbs the energy from the incident light which would be totally reflected without the metal film. This phenomenon is also called surface plasmon resonance, providing an effective means of measuring the optical constant of flowing liquid in real time.

The SPR angle of an incident light depends on the refractive index of the probed samples at the solid-liquid interface. The detection output refers to the change of the SPR angle. The technologies of incident-angle variation and angle-dependent image detection are required to perform a high precision measurement. Instead of varying the angle, wavelength interrogation and intensity measurement are normally applied. SPR sensors based on wavelength interrogation and intensity detection are less precise than the SPR sensors applying angular interrogation[3,4].

In this paper, we suggest a novel scheme using the EO modulation[5] to replace the angular detection or the wavelength variation. This is achieved by coating with nonlinear optical materials that interact with the surface plasmon. The scheme determines the SPR angle using an electrical signal that is directly readable. Canceling the angle-reading mechanism reduces the sensor size while providing the potential of array sensing as well as maintaining the precision of angular interrogation. Moreover, multiple light sources for differential measurements are one of the feasible options.

SPR sensors containing dielectric-metal-dielectric multilayer have been considered to improve the sensing sensitivity, the spectral resolution and even have the capability of detecting the sample anisotropy[6]. Recently, Toyama *et al*[7] applied metal-dielectric-metal multilayer for higher SPR sensing stability using the difference between TM- and TE-resonance angles. A configuration of metal-dielectric-ITO, *i.e.*, indium tin oxide reported by Teng *et al*[8] in 1990 became more or less a standard method to study the EO character of thin films. All the multilayer structures mentioned above are suitable for the application of the EO modulated SPR sensor. We present in this paper a detailed analysis of these possible configurations including some considerations from the manufacturing side.

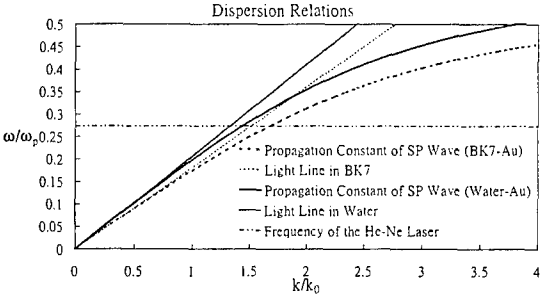

Figure 1: Dispersion relations (eq. 1) of the surface plasmons on the interface between a semi-infinite dielectric medium (BK7, n=1.515 or water, n=1.33) and a semi-infinite metal (Au, n=0.163+i3.52). The straight lines are the light lines in the media of BK7 glass and water, respectively. The wavelength of the He-Ne laser is 632.8nm.

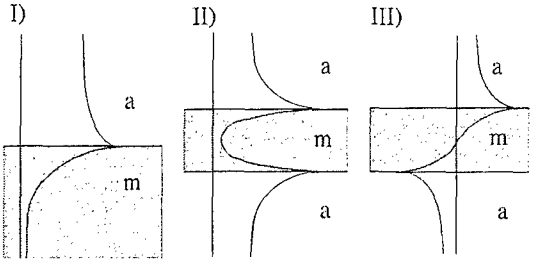

Figure 2: Distribution of the transverse magnetic field parallel to the surface on which the surface plasmon propagates. The characters m and a denote the metal and the dielectric medium, respectively. I) Plasmon fields near the interface between a semi-infinite metal and a semi-infinite dielectric medium. II) Long-range mode on a metal slab. III) Short-range mode on a metal slab.

2. SURFACE PLASMON

We consider firstly a simple interface between semi-infinite dielectric and semi-infinite metal. A charge-density oscillation associated with electromagnetic wave evanescently decaying into both media may propagate along the interface. The dispersion relation of this surface plasma wave in figure 1 is given by the equation[9]:

$$\omega = c\, k_{SP} \sqrt{\frac{1}{\varepsilon_m} + \frac{1}{\varepsilon_a}}. \qquad (1)$$

Considering only metals in the SPR application[10], the dielectric constant ε_R has a large negative value, as the oscillation frequency is less than the plasma frequency. In this case, the equation (2) indicates that the propagation constant of the surface plasmon is always larger than the propagation constant of light in the associated dielectric. A finite value of ε_I denotes that the metal is dissipative. k_I determines the exponential decrease of the oscillation intensity. Assuming $k_R >> k_I$ that implies $-\varepsilon_R > \varepsilon_a$, we have

$$k_R \approx \sqrt{\varepsilon_a}\, k_0 \sqrt{1 + \frac{\left|\varepsilon_a^2 + \varepsilon_R \varepsilon_a\right|}{\left|\varepsilon_m + \varepsilon_a\right|^2}} \tag{2}$$

and

$$k_I = \frac{1}{2} \frac{\varepsilon_a^2 \varepsilon_I}{k_R} \frac{k_0^2}{\left|\varepsilon_m + \varepsilon_a\right|^2}. \tag{3}$$

Here, we note in the equation (3) that k_I is proportional to ε_I. It demonstrates that the damping is due to the energy loss in the metal[11].

The evanescent wave decays faster in the metal than in the dielectric. These decay rates γ_m and γ_a are known as the extinction coefficients which are given by the equation

$$\gamma_m = k_0 \mathrm{Re}\left(\frac{\varepsilon_m}{\sqrt{\varepsilon_m + \varepsilon_a}}\right) \tag{4}$$

and

$$\gamma_a = k_0 \mathrm{Re}\left(\frac{\varepsilon_a}{\sqrt{\varepsilon_m + \varepsilon_a}}\right) \tag{5}$$

for the metal and dielectric, respectively, where the symbol of Re means the real part of the number. As ε_a increases, γ_m and γ_a increase too. Figure 2-I denotes this distribution of the transverse magnetic field schematically.

Secondly, we consider a metal slab of thickness d bonded on both sides by the identical medium with the dielectric constant ε_a. When the thickness of metal slab is large with the condition $d\gamma_m >> 1$, the surface plasmons propagate on each side of the interfaces with the same speed and the same damping rate. Each one of these two surface plasmons generates evanescent waves into the metal slab and into the dielectric. As the metal thickness decreases, the decoupled surface plasmons interact with each other. Consequently, the degenerate dispersion relations of the surface plasmons split into one longe-range and one short-range mode[9,11,12].

The case that surface plasmons propagate in anti-phase[9] is known as the long-range mode that has an identical magnetic field distribution on both metal-dielectric interfaces (fig. 2-II). In the short-range case, surface plasmons propagate in phase. The transverse magnetic field distribution are anti-symmetrical referred to central line of the metal as shown in figure 2-III.

The long-range mode has higher phase velocity and lower damping rate than the short-range mode. The damping rate of the long-range mode goes to zero with a phase velocity approaching the light speed in the dielectric ($k_R \to \sqrt{\varepsilon_a}\, k_0$), as the metal thickness vanishes[11,12]. Because of its long propagation distance, the mode with a symmetric magnetic field distribution is called the long-range surface-plasmon mode. As the thickness of the metal slab decreases, the decay rate in the dielectric of long-range mode proportionally decreases ($\gamma_a^2 \approx k_R^2 - \varepsilon_a k_0^2$). In the case of the long probing length, the long-range mode is not useful for SPR sensing without a proper modification. The short-range mode has strong field inside the metal associated with a fast decay outside. As the film thickness decreases, the phase velocity diverges, the damping of the plasmon becomes very strong, and the evanescent waves in both sides decay very fast.

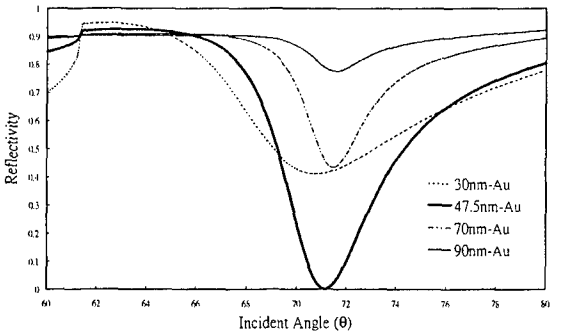

Figure 3: Reflectivity of a configuration of prism-Au-water. As the Au-film thickness decreases, the angle of minimal reflectivity increases slightly

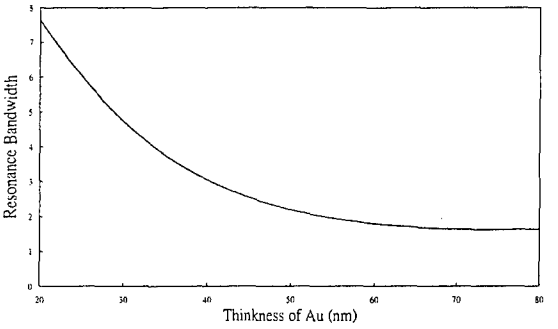

Figure 4: Resonance bandwidth (not to scale) decreases, as the Au-film thickness decreases. This curve indicates that the excited plasmon is a short-range mode.

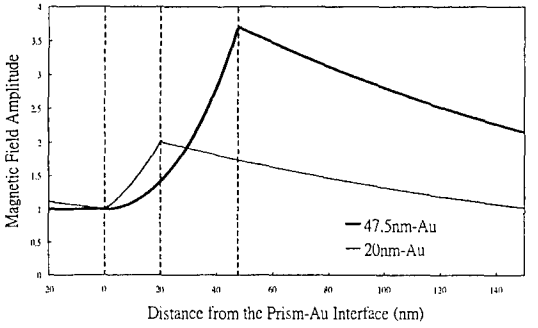

Figure 5: Intensity plot of prism-Au-water configurations. The transverse magnetic fields are normalized to 1 at the prism-Au interface. The plot starts from the BK7 at 20 nm to the interface prism-Au. The plasmons are excited on the prism-water interface where the field energy is stored to a maximal value. The thickness' of the Au-film calculated here are 20 nm and 47.5nm.

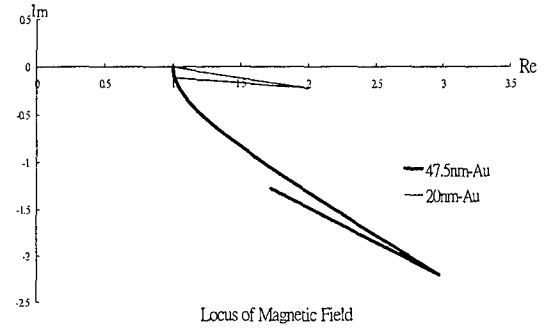

Figure 6: Locus plots of the complex field associated to Fig. 5. The complex number (1,0) presents the interface of prism-Au. The locus's move down- and rightward in the Au film and turns back to the origin point in the water. These plots demonstrate that the surface plasmons are the short-range mode whose field is almost antisymmetric for both cases of 20 nm and 47.5 nm gold.

Finally, we consider an asymmetric configuration of a metal slab bounded by semi-infinite dielectric media with different dielectric constants. They are ε_a and ε_b referred to the upper medium a and the lower medium b. Assuming $\varepsilon_a > \varepsilon_b$, which is commonly used for the SPR sensor in the prism coupling method also known as the Kretschmann configuration[13]. The plasmons propagate in different speeds with their own dispersion functions. As long as the slab thickness is large enough, they behave like the equation (1). As the metal thickness decreases, the interaction between the surface plasmons becomes stronger and leads to complicate solutions, especially in the case when the dielectric constants are close[14]. There are four kinds of possible solutions for an asymmetric configuration[11,14], *i.e.*, the modes of symmetric bound (nonradiative), symmetric leaky (radiative), antisymmetric bound, and antisymmetric leaky (referred to the transverse magnetic field distribution). The nonradiative modes can be excited by the ATR method[9].

A commonly applied configuration of the SPR sensor is the glass BK7-Au-water system with refractive indices at the He-Ne laser (λ =0.6328 μm) of 1.515/ 0.163 + i3.52/ 1.33, respectively. A gold thickness of 50 nm is commonly applied. The plasmon locates at the stable working point as an antisymmetric mode described by Brurke *et al*[11]. The damping constant k_I is originated not only from the dissipation in the metal but also from the radiation loss into glass BK7[9]. As shown in the fig. 1, the working point of plasmon excitation is the intersection between the line of the laser frequency and the dispersion relation of the Au-water surface plasmon. The Au-BK7 plasmon is impossible to be excited by the coupling prism method, since its propagation constant is always larger than the propagation constant of the light line in BK7 (eq, 2). The propagation constant of the Au-water plasmon is less than the propagation constant of the laser light in BK7 at the working point (fig.1), therefore the reflecting wave from the plasmon back into BK7 is radiative. In this case, we observed an increasing damping associated with a decrease in gold thickness (Fig. 3,4). The resonance angle (~71 degree) is far from the critical angle of the BK7-water

interface (61.4 degree). The evanescent wave in the water decays relative fast. The SPR reflectivity calculated in this paper are analyzed using the complex Fresnel calculations[15,16].

Figure 5 illustrates the intensity of the magnetic field along the direction from the prism BK7 into the water for two configurations, *i.e.*, 47.5 nm- and 20 nm- gold film. The reflex points of the field curves indicate the charge density accumulated on the metal surface. The peaks at the gold-water interfaces denote that the surface plasmons are excited there as an active interface. The charge density across the gold film at the prism-gold interface is an image charge carrying the same sign. Figure 6 shows a phase lag between the excited plasma wave and its image due to the lower phase velocity at the image side. However, this excitation is similar to a short-range mode where the magnetic field distribution is more or less like the mode illustrated in fig. 2-II.

3. MULTILAYER STRUCTURE

There are conventionally two configurations to excite the surface plasmon by the coupling prism method, *i.e.*, the Kretschmann configuration[13] and the Otto configuration[17]. It is convenient to replace the air gap in the Otto configuration by a low refractive dielectric, which leads to the multilayer structure.

One matched multilayer configuration is chosen to obtain symmetric structure, *i.e.*, prism-index matching liquid (n=1.4564)-Ag-fused silica (n=1.4569)[18]. A long-range surface-plasmon mode was measured on very thin silver film in this symmetric configuration[18]. Kessler *et al*[19] extended this multilayer configuration via replacing the matching layers by Teflon. In their study, the sharp absorption bands were found for both TM and TE incident light. Salamon *et al*[16] demonstrated that both the reflectivity curves of TM- and TE-waves are applicable to the BIA system. Kessler *et al*, also found the long-range surface excitation propagating on a highly lossy active layer instead of a highly conductive metal layer. The idea of a lossy active layer was originally reported by Yang *et al*[20]. Recently, another multilayer configuration was reported by Toyama *et al*[7] with double active metal layers. In this special multilayer configuration, The TE-resonance angle is not sensitive to the sample. On the contrast, the TM resonance angle is sensitive and tunable by changing layer thickness.

Figure 7 shows a multilayer structure of the Toyama type[7]. Two metal layers sandwich a dielectric medium that is considered to be an EO material in this paper. The EO material is highly refractive in general cases. Assuming the refractive index of a polymer EO layer is 1.63. The reflectivity curves of TM- and TE-waves have very similar behavior scanning the incident angle from 0 to 90 degree, as the thickness of the EO layer is around 400 nm. Each one performs two resonance angles. One of them is less than the critical angle and the other is greater than the critical angle. The TM-resonance in the total reflection region (fig. 8) has a bandwidth similar to the resonance in figure 3.

Assuming that the reflectivity curve at the resonance angle is proportional to

$$R \approx \min + \mathrm{curv} \times (\theta - \theta_R)^2 . \tag{6}$$

We can steer the angle by varying the refractive index of the EO layer. A general definition of the sensitivity is the reflectivity change referred to the index change at the angle where the half reflectivity occurs comparing to the resonance minimun[10]. We define the sampling and steering sensitivity expressed in the following equations:

$$S_P = \frac{dR}{d\theta}\frac{d\theta}{dn_P} \tag{7}$$

and

$$S_S = \frac{dR}{d\theta}\frac{d\theta}{dn_S} \tag{8}$$

with

$$\frac{dR}{d\theta} = \sqrt{2\mathrm{curv}(1-\min)} \tag{9}$$

that is taken at the angle of the half bandwidth[10]. The angle change referred to the sample index change is calculated numerically by varying the sample index slightly from the water index. The sample layer is set to be 5 nm thick attached between Au-water. The formulae of (7~9) are suitable for the feedback application of the EO modulation as described later in the section 4. These definitions of sensitivities do not include the feature of the apparatus such as the diffraction effects associated with the finite width of the laser beam[10,18]. In the following calculations, we try to avoid the very sharp resonance whose bandwidth is less than 0.05 degree[18].

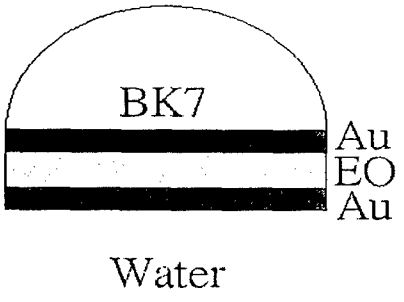

Figure 7: Multilayer structure of coupling prism method using two identical gold-films to sandwich the EO layer. The BIA layer should be attached to the gold-water interface. The calculations apply the He-Ne laser with the wavelength of 632.8 nm.

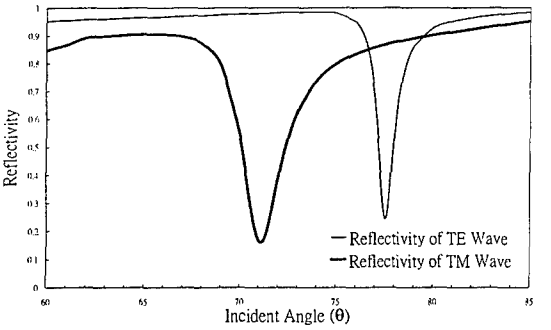

Figure 8: Reflection curves of the TE- and TM-resonance. Both resonance have angles greater than the critical angle of prism-water. The calculated configuration is 30nm Au-400 nm EO-30nm Au.

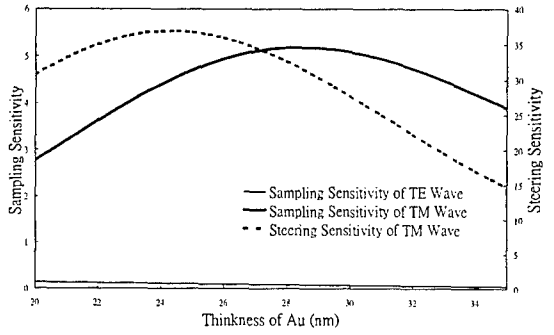

Figure 9: Sampling sensitivities and steering sensitivity of the TE- and TM-resonance illustrated as functions of the gold thickness. The sampling sensitivity of TE-resonance is very low, as shown here. Its associated steering sensitivity is not illustrated. The thickness of the EO layer used in this calculation was 400 nm.

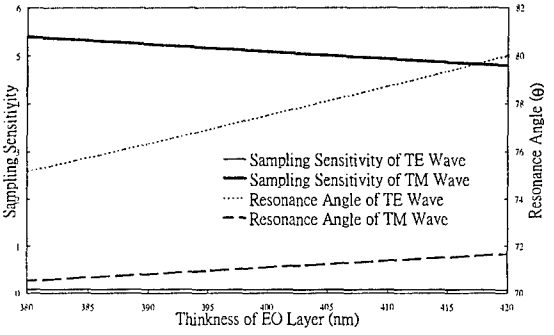

Figure 10: Sampling sensitivities and resonance angles of the TE- and TM-resonance illustrated as functions of the EO thickness. The thickness of gold-films calculated here is 30 nm. As the EO thickness increases, the resonance angles increase, but the sampling sensitivities decrease.

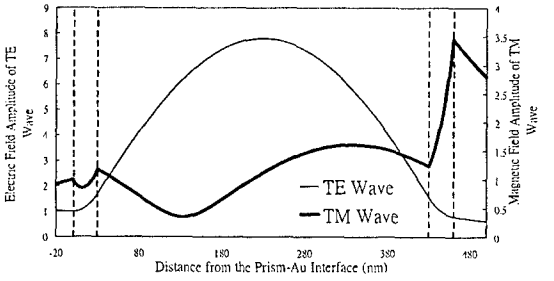

Figure 11: Transverse field distributions of the TE- and the TM-resonance. Two gold films locate at the sections of 0-30 nm and 430-460 nm. The excited plasmon locates at the gold-water interface at 460 nm. The field distributions in the EO layer are symmetric and antisymmetric referred to the TE- and TM-resonance. The plot starts from the BK7 at 20 nm to the interface.

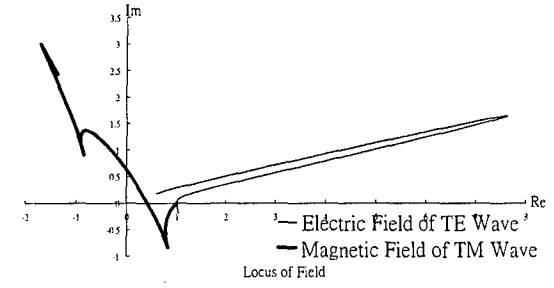

Figure 12: Locus plots of the complex transverse fields of the TE- and TM-resonance associated to their field plots of Fig. 11. The deflections of TM locus denote the charge density accumulation at the metal-dielectric interfaces. The plasmon has a symmetrical field distribution in the first gold film but antisymmetrical in the second gold film referred to each metal center.

Figure 9 and figure 10 illustrate the functional parameters of the multilayer SPR sensor shown in figure 7. The sampling sensitivity of the TE-resonance is very low as described in Toyama's configuration[7]. In this case, we can apply a differential measurement between the resonance angles of the TM- and the TE-wave. Figure 9 shows that the TM-sampling and TM-steering sensitivities have different maximal values, as the gold thickness increases. The TM-steering sensitivity is low

compared to the TE-steering sensitivity due to the TM-phase change in the EO layer. The TE steering sensitivity is very high because of the in-phase high-field distribution in the EO layer (fig. 11). We found that the field drop at the second gold film causes a low TE-sampling sensitivity. The TE-steering sensitivity is not shown in Fig. 9 due to its low sampling sensitivity. The probing depth is directly related to the resonance angle (fig. 10). One chooses large resonance angle for the short probing depth and vice versa. An optimal choice of these parameters depends on the applications. The TM-sampling sensitivity decreases due to the field reduction at the water interface, as the EO thickness increases. The surface plasmon on the Au-water interface is excited and characterized by a peak of the transverse field (fig. 11). High field is preferred for a high sampling sensitivity. The associated locus plot in figure 12 demonstrates that the TM-phase changes sign in the EO layer. We found that the magnetic fields are symmetric in the upper gold film but antisymmetric in the lower gold film. Note that the charge densities are symmetric between the gold films across the EO layer. We like to remind the readers again that all field calculations are normalized to the prism-gold interface with the complex number (1,0).

According to the description in section 2, we find significant long-range plasmon coupling through the three interfaces on which plasmon excitations perform similar dispersion relations, as the dielectric constant of the EO layer approaches the water index. The magnetic field distributions in the second gold film become symmetric (fig. 13 and 14). The resonance bandwidths are smaller and resonance fields are higher, if we compare these results with the cases of figures 9 ~12. However, the probing evanescent waves become long extended. Note that plasmons on different interfaces are excited in the configurations with EO indices changing from 1.4 to 1.33.

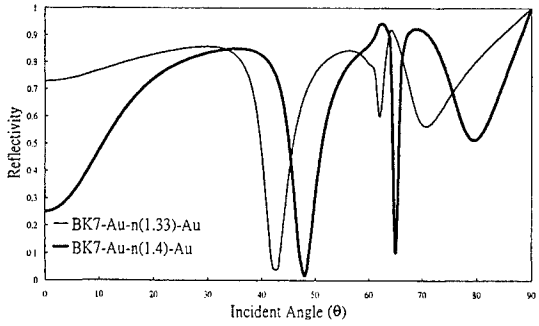

Figure 13: Reflectivity curves of the TM-wave configured with the refractive index of the EO layer to be 1.33 (water) and 1.4. The resonance angles are close to the critical angle (61 degrees) of prism-water. The parameters used in this calculation are 25 nm AU - 600 nm EO layer – 25 nm Au.

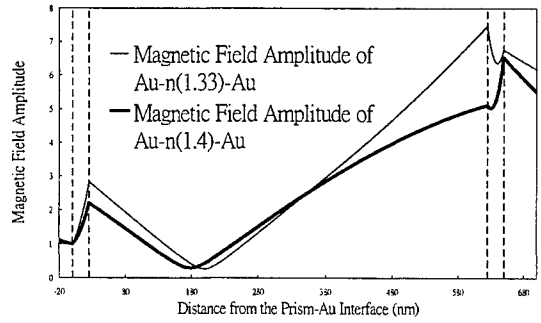

Figure 14: Magnetic field of TM-wave associated to the sharp resonance near the critical angle in Fig. 13. Note that the plasmons at different interface were excited. Note that the second gold film has a symmetric field distribution. The plot starts from the BK7 at 20 nm to the interface.

In this paragraph, we describe the TM-resonance shown in figure 15 with a typical gold thickness of 50 nm. As the EO layer (index=1.63) is less than 20 nm, the reflectivity curve has the same behavior as the configuration discussed in figure 3. This mode is not interesting due to its low sampling sensitivity. As the EO thickness increases to 280 nm, a sharp resonance appears. The TM-resonance angle increases from the critical angle of 61 degrees to 90 degrees as the EO thickness increases from 280 nm to 530 nm. On the other hand, the TE-resonance firstly appears at 130 nm with an angle close to the critical angle. The TE-resonance disappears around 380 nm characterized by its angle passing 90 degrees. The resonance angles of both TM- and TE-waves move periodically, as the EO thickness increases. One can choose the EO thickness to obtain either one resonance between TM- and TE-waves or both resonance (fig. 16). The resonance angles are tunable by the EO thickness. Both types of resonance are sensitive from the viewpoint of the BIA system. The TE-resonance performs very high sensitivities in steering as well as in sampling (fig. 17), since the fields are high and in-phase in the EO layer (fig. 19). The TE-sensitivities decrease due to less energy transferred into the resonant waveguide of the EO layer, as the thickness of the gold film increases (fig. 17). On the contrast, the TM sensitivities increase due to the growth of plasmon excitation (same behavior as fig. 5), as the thickness of the gold film increases (fig. 17). The coupling prism excitation of this mode is difficult to interpret, because the plasmon should have a propagation constant greater than that of the light line in BK7due mainly to the higher EO index (1.63/EO>1.515/BK7). Consequently, the ATR method can not excite the plasmon. However, the EO layer is finite and works like a waveguide coupling the field from low-index side of sample to metal by a standing wave. This leads to the coupled plasmon-waveguide resonance excitation[6]. The field and locus plots in figure 19 and 20 indicate two different types of TE- and TM-resonance in the EO layer. One performs symmetric field-distribution and the other performs antisymmetric field-distribution referred to central line of the EO layer.

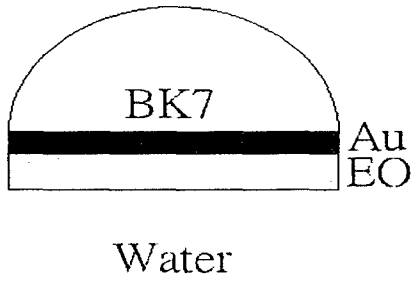

Figure 15: Multilayer structure of coupling prism method using an EO layer. The BIA layer should be attached to the EO-water interface. The calculations apply the He-Ne laser with the wavelength of 632.8 nm.

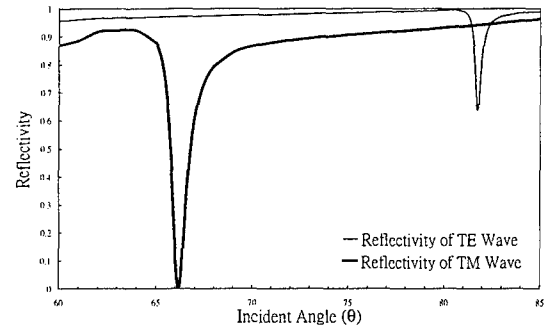

Figure 16: Reflection curves of the TE- and TM-resonance. Both the resonance angles are greater than the critical angle of prism-water. The configuration calculated here is BK7-50 nm Au-350 nm EO-water.

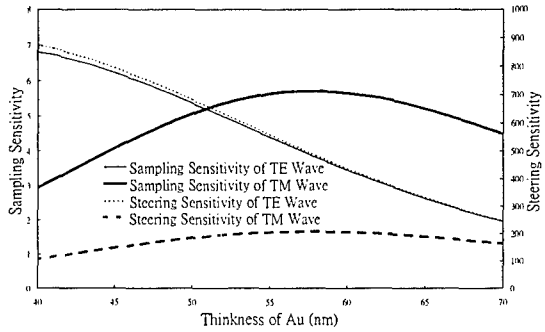

Figure 17: Sampling sensitivities and steering sensitivities of TE- and TM-resonance illustrated as functions of the gold thickness. Both the sampling and steering sensitivities of the TE-resonance are very high compared to those sensitivities of the TM resonance. The thickness of the EO layer used in this calculation is 350 nm.

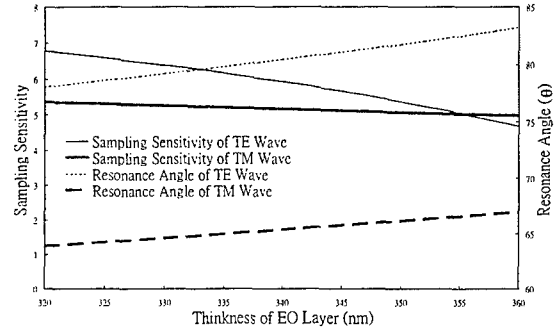

Figure 18: Sampling sensitivities and resonance angles of the TE- and TM-resonance illustrated as functions of the thickness of the EO layer. The thickness of the gold film used in the calculations is 50 nm. As the EO thickness increases, the resonance angles increase, but the sampling sensitivities decrease.

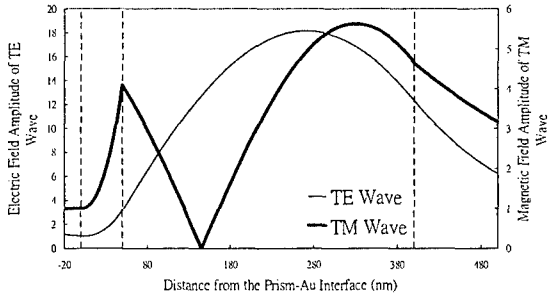

Figure 19: Transverse field distributions of the TE- and the TM-resonance. The thickness of the gold film and the EO layer used in the calculation are 50 nm, 350 nm, respectively. The plasmon excited locates at the gold-EO interface. The field distributions in the EO layer are symmetric and antisymmetric referred to the TE- and TM-resonance, respectively.

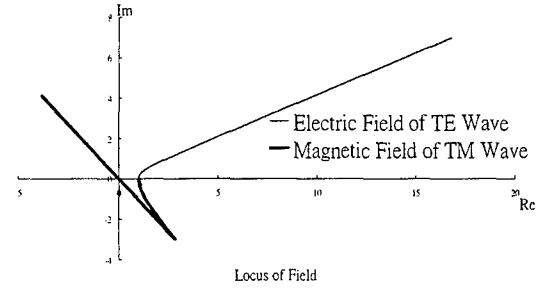

Figure 20: Locus plots of the complex transverse fields of the TE- and TM-resonance associated to the field plots in Fig.19. The deflections of TM locus denote the charge density accumulation at the metal-dielectric interfaces. The plot starts from the BK7 at 20 nm to the interface.

According to the calculation of Zervas[14], we can find the long-range surface-plasmon, as the EO index approaches the index of BK7. Figure 21 illustrates this result to be a long-range mode. The resonance is very sharp that indicates that the propagation distance is very long. Figure 22 illustrates the associated field distribution. For such a high field at the interface, several papers[21,22,23] considered nonlinear effects of the material. It should be carefully studied, especially in our case.

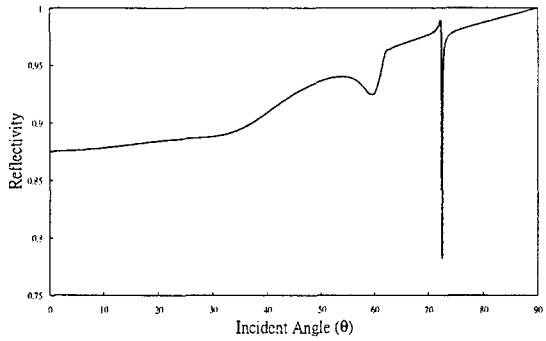

Figure 21: Reflectivity curves of the TM-wave configured in the same geometry shown in Fig. 19 but with a EO index to be 1.5 close to the index of the prism.

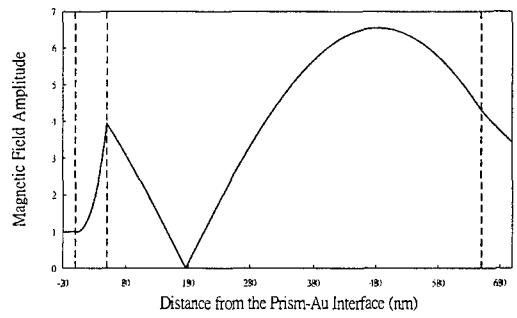

Figure 22: Magnetic field associated to the sharp TM-resonance in Fig. 21. The configuration is BK7-50 nm Au-600 nm EO-water. The plot starts from the BK7 at 20 nm to the interface.

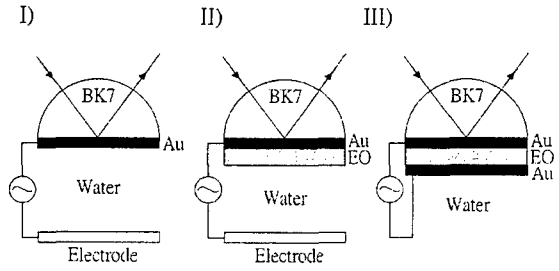

Figure 23: Three possible configuration of EO modulation. Figures I and II have an electrode in the water. The BIA sample is considered to coat on the metal-water interface.

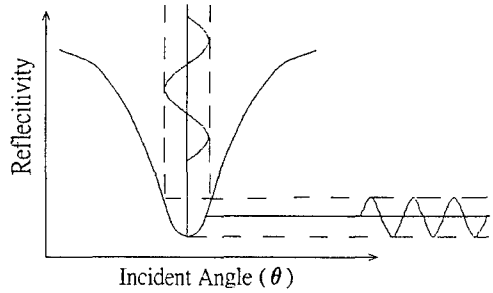

Figure 24: Using the electric signal to modulate the EO layer. The second harmonic results in the reflectivity, as the incident angle match the resonance angle.

4. ELECTRO-OPTIC MODULATION

Loulergue *et al*[24] investigated in 1988 how a static electrical field affects a Langmuir-Blodgett film (single molecular layer, thickness 2.5nm – 3nm) of an azo dye. In this study, the dye layer has been deposited on an Ag film and also measured ts reflectivity has been measured versus applied field. An angle change of 3 degrees for an applied field of 9 volts has been reported. A simple EO-modulation scheme is considered using water as the EO material (figure 23-I). The charge density in the double layer induced by the current flow at the metal-water interface attributes to the modulation of the SPR sensing[25]. This scheme has the drawbacks that the modulation response is not linear and slow. Furthermore, the electric current is large and passes through the BIA sample.

Figure 21-II sketches the improved scheme to replace the double layer by the EO layer. Recent progress in the EO polymers[26,27] provides the fabrication capability of integrated optic devices that is suitable for the SPR array sensing. Although the modulation speed of polymer can be driven up to the GHz range, this scheme should stay in the low frequency region to avoid current flow in the water.

The third scheme of figure 21-III avoids all drawbacks of the previous two. The modulation field appears only between the gold films. The film thickness is not too thin to fabricate. Even the upper gold layer can be replaced by silver that provides a further improvement of sensitivities without worrying about the degradation[7].

Assuming that a sinusoid electric field of frequency f_m applies on the EO layer and the incident angle of light is at the resonance angle. Figure 24 shows that the photo detector will generate a second harmonic signal. As long as the incident angle matches the resonance angle, there is no signal of the f_m modulation frequency. We consider a feedback loop to cancel the modulation frequency using a dc bias voltage between the electrodes. The dc bias is directly readable with a high response speed. There is no electrode in the water. Therefore, an integrated circuit with this biochip can drive the modulation speed up to multi-GHz range. A high S/N ratio and a very fast feedback loop with high gain can be obtained. It is possible to realize the array and the differential sensing on the chip.

5. DICUSSION

An ideal design of the SPR sensor using EO modulation described in this paper should have the following features:

1. High sensitivity to probe the BIA sample,
2. Capability of array sensing with single incident light,
3. Capability of multiple wavelength of the incident light,
4. Differential measurement to increase the precision,
5. High real-time detecting speed,
6. High S/N ratio for the high resolution sensing,
7. Tunable probing depth,
8. Large dynamic range of EO modulation,
9. Stable working point with large manufacturing tolerance,
10. Small size and easy to fabricate.

We discussed the physics of the surface-plasmon excitation in section 2. Two major configurations of figures 23-II and 23-III were considered realizing the features mentioned above. The configuration of metal-dielectric-ITO reported by Teng *et al*[8] is less favorable because of its low dynamic range of the EO steering. The EO layer should be placed as close as possible to the plasmon surface where the field is high. A long-range surface-plasmon with tunable resonance angle is preferred due to its high resolution and high field concentration. However, a very sharp bandwidth might not increase the resolution due to the divergence of the laser light. But, the strong resonance field certainly leads to the required features in the aspects of large modulation dynamic range and high sampling sensitivity. We choose a polymer as EO martial because of its low refractive index. The index of EO polymer is unfortunately higher than the index of prism. Although we can choose the high refractive prism in our application, it is not favorable due to its high price and low popularity. In this paper, we found a long-range mode that is usually not considered to be possible but occurred only in a strong coupling configuration.

The configuration of figure 23-II has the advantages of high sampling sensitivity, large dynamic range and possibility of stereo detection. However, the electrode in the water will inhibit the modulation speed. The nonlinear modulation of the double layer will cause further problems. The polymer might also degrade due to ac charging in the water solution.

The optimal choice of a EO configuration seems to be figure 23-III so far. The detecting speed is high, the metal layer is not too thin, and almost all the required features listed above are satisfied. We are sure that there is still plenty of room to improve this configuration.

6. CONCLUSION

We suggested a novel detection schemes to replace the mechanism of the angular measurements or wavelengths variation using an EO coating on the plasmon active interface to perform EO modulation. This method determines the SPR angle using an electrical signal that is directly readable. Canceling the angle-reading mechanism reduces the sensor size while providing potential of array sensing as well as maintaining the precision of angular interrogation. Moreover, multiple light sources for array and differential measurements are one of the feasible options.

ACKNOWLEDGEMENT

The National Health Research Institutes supported this work within the National Science and Technology Program of Pharmaceuticals and Biotechnology. Grants number is NSC-89-2323-213-001. The authors thank Miss M.-F. Tsai for the search of references.

REFERENCES

1. G. J. Sprokel and J. D. Swalen, "The Attenuated Total Reflection Method", chapter 4, *Handbook of Optical Constants of Solids II*, Edited by E. D. Palik, Academic Press, INC., 1991.
2. B. Liedberg, C. Nylander, I. Lundström, "Surface plasmons resonance for gas detection and biosensing", Sensors and Actuators **4**, pp. 299-304, 1983.
3. J. Homola, S.S. Yee, G. Gauglitz, "Surface plasmon resonance sensors: review", Sensors and Actuators **B54**, pp. 3-15, 1999.
4. J. Homola, I. Koudela, S.S. Yee, "Surface plasmon resonance sensors based on diffraction gratings and prism couplers: sensitivity comparison", Sensors and Actuators **B54**, pp. 16-24, 1999.
5. B. E. A. Saleh, M. C. Teich, "Electro-optics", Chapter 18, *Fundamentals of photonics*, Jihn Wiley & Sons, 1991.

6. Z. Salamon, H. A. Macleod, and G. Tollin, "Coupled plasmon–waveguide resonators: A new spectroscopic tool for probing proteolipid film structure and properties", Biophys. J. **73**, pp. 2791-2797, 1997.
7. S. Toyama, N. Doumae, R. Usami, K. Horikoshi, and Y. Ikariyama, "Ag-SiO_2-Au Thin film for the stabilization of the signal of SPR-based immunosenser" Transducer '99, Sendai, Japan, pp. 1344-1346, 1999.
8. C. C. Teng and H. T. Man, "Simple reflection technique for measuring the electro-optic coefficient of poled polymers", Appl. Phys. Lett. **56** (18), pp. 1734-1736, 1990.
9. H. Raether, "Surface plasma oscillations and their applications", Phys. Thin Films, **9**, pp. 145-261, 1977.
10. H. E. de Bruijn, R. P. H. Kooyman, and J. Greve, "Choice of metal and wavelength for surface-plasmon resonance sensors: some considerations", Applied Optics, 31(4), pp. 440-442, 1992.
11. J. J. Burk and G. I. Stergeman, T. Tamir, "Surface-polariton-like waves guided by thin, lossy metal films", Phys. Rev. B, **33**, pp. 5186-5201, 1986.
12. D. Sarid, "Long-range surface-plasma wave on very thin metal films", Phys. Rev. Lett. **47**, pp. 1927-1930, 1981.
13. E. Kretschmann, H. Raether, "Radiative decay of non-radiative surface plasmon excited by light", Z. Naturforsch. **23A**, pp. 2135-2136, 1968.
14. M. N. Zervas, "Surface plasmon-polariton waves guided by thin metal film", Opt. Lett. **16**(10), pp. 720-722, 1991.
15. W. N. Hansen, "Electric fields produced by propagation of plane coherent electromagnetic radiation in a stratified medium", J. Opt. Soc. Am. 58, pp. 380-390, 1968.
16. H. A. Macleod, *Thin-film optical filter*, Ch. 2, Adam Hilger Ltd, Bristol, 1986.
17. A. Otto, "Excitation of surface plasma waves in silver by the method of frustrated total reflection", Z. Physik **216**, pp. 398-410, 1968.
18. J. C. Quail, J. G. Rako, and H. J. Simon, "Long-range surface-plasmon modes in silver and aluminum films", Opt. Lett. **8**(7), pp. 377-379, 1983.
19. M. A. Kessler, E. A. H. Hall, "Multilayered structure exhibiting long-range surface exciton resonance", Thin Solid Films, **272**, pp. 161-169, 1996.
20. F. Yang, J. R. Sambles, and G. W. Bradberry, "Long-range coupled surface exciton polaritons", Phys. Rev. Lett. **64**, pp. 559-562, 1990.
21. D. Sarid, R. T. Deck, and J. J. Fasano, "Enhanced nonlinearity of the propagation constant of a long-range surface plasma wave",J. Opt. Soc. Am., **72**(10), pp1345-1347, 1982.
22. R. T. Deck, D. Sarid, "Enhancement of second-harmonic generation by coupling to long-range surface plasmons", J. Opt. Soc. Am., **72**(12), pp1613-1617, 1982
23. G. I. Stergeman and J. J. Burk, D. G. Hall, "Nonlinear optics of long-range surface plasmons", Appl. Phys. Lett, **41**(10), pp. 906-908, 1982.
24. J. C. Loulergue, M. Dumont, Y. Levy, P. Robin, J. P. Pocholle and M. Papuchon, *Thin Solid Films* **160**, 399, 1988.
25. Badia, S. Arnold, V. Scheumann, M. Zizlsperger, J. Mack, G. Jung W. Knoll, "Probing the electrochemical deposition and/or desorption of self-assembled and electropolymerizable organic thin films by surface plasmon spectroscopy and atomic force microscopy", Sensors and Actuators **B54**, pp. 145-165, 1999.
26. J. G. Grote, "Design and fabrication of nonlinear optic polymer integrated optic devices", chapter 16, *Electrical and optical polymer systems*, MARCEL DEKKER, INC., New York, 1998.
27. L. R. Dalton, "Polymers for electro-optic modulator waveguides", chapter 19, *Electrical and optical polymer systems*, MARCEL DEKKER, INC., New York, 1998.